Inorg. Chem. **2002**, *41*, 1795–1806

A Dinuclear Manganese(II) Complex with the $\{Mn_2(\mu\text{-}O_2CCH_3)_3\}^+$ Core: Synthesis, Structure, Characterization, Electroinduced Transformation, and Catalase-like Activity

Isabel Romero,[1a,b] Lionel Dubois,[1c] Marie-Noëlle Collomb,*[,1b] Alain Deronzier,*[,1b] Jean-Marc Latour,*[,1c] and Jacques Pécaut[1c]

Departament de Quimica, Universitat de Girona, Campus de Montilivi, E-17071 Girona, Spain, Laboratoire d'Electrochimie Organique et de Photochimie Rédox, UMR CNRS 5630, Université Joseph Fourier, Grenoble 1, BP 53, 38041 Grenoble Cedex 9, France, and DRFMC, Laboratoire de Chimie Inorganique et Biologique, UMR CEA-CNRS-UJF 5046, CEA-Grenoble, 38054 Grenoble Cedex, France

Received July 9, 2001

Reactions of $Mn^{II}(PF_6)_2$ and $Mn^{II}(O_2CCH_3)_2 \cdot 4H_2O$ with the tridentate facially capping ligand *N*,*N*-bis(2-pyridylmethyl)-ethylamine (bpea) in ethanol solutions afforded the mononuclear $[Mn^{II}(bpea)](PF_6)_2$ (**1**) and the new binuclear $[Mn_2^{II,II}(\mu\text{-}O_2CCH_3)_3(bpea)_2](PF_6)$ (**2**) manganese(II) compounds, respectively. Both **1** and **2** were characterized by X-ray crystallographic studies. Complex **1** crystallizes in the monoclinic system, space group $P2_1/n$, with $a = 11.9288(7)$ Å, $b = 22.5424(13)$ Å, $c = 13.0773(7)$ Å, $\alpha = 90°$, $\beta = 100.5780(10°)$, $\gamma = 90°$, and $Z = 4$. Crystals of complex **2** are orthorhombic, space group $C222_1$, with $a = 12.5686(16)$ Å, $b = 14.4059(16)$ Å, $c = 22.515(3)$ Å, $\alpha = 90°$, $\beta = 90°$, $\gamma = 90°$, and $Z = 4$. The three acetates bridge the two Mn(II) centers in a $\mu_{1,3}$ syn–syn mode, with a Mn–Mn separation of 3.915 Å. A detailed study of the electrochemical behavior of **1** and **2** in CH_3CN medium has been made. Successive controlled potential oxidations at 0.6 and 0.9 V vs Ag/Ag^+ for a 10 mM solution of **2** allowed the selective and nearly quantitative formation of $[Mn^{III}_2(\mu\text{-}O)(\mu\text{-}O_2CCH_3)_2(bpea)_2]^{2+}$ (**3**) and $[Mn^{IV}_2(\mu\text{-}O)_2(\mu\text{-}O_2CCH_3)(bpea)_2]^{3+}$ (**4**), respectively. These results have shown that each substitution of an acetate group by an oxo group is induced by a two-electron oxidation of the corresponding dimanganese complexes. Similar transformations have been obtained if **2** is formed in situ either by direct mixing of Mn^{2+} cations, bpea ligand, and CH_3COO^- anions with a 1:1:3 stoichiometry or by mixing of **1** and CH_3COO^- with a 1:1.5 stoichiometry. Associated electrochemical back-transformations were investigated. **2**, **3**, and the dimanganese $[Mn^{III}Mn^{IV}(\mu\text{-}O)_2(\mu\text{-}O_2CCH_3)(bpea)_2]^{2+}$ analogue (**5**) were also studied for their ability to disproportionate hydrogen peroxide. **2** is far more active compared to **3** and **5**. The EPR monitoring of the catalase-like activity has shown that the same species are present in the reaction mixture abeit in slightly different proportions. **2** operates probably along a mechanism different from that of **3** and **5,** and the formation of **3** competes with the disproportionation reaction catalyzed by **2**. Indeed a solution of **2** exhibits the same activity as **3** for the disproportionation reaction of a second batch of H_2O_2 indicating that **3** is formed in the course of the reaction.

Introduction

Hydrogen peroxide is a byproduct of aerobic respiration; nevertheless in the presence of reductive metals (Fe(II) or Cu(I)), it can be converted to hydroxyl radicals whose deleterious effects on cell components is well documented.[2,3] Therefore all living cells have devised a sophisticated machinery to suppress or at least control H_2O_2 production. The catalase enzymes which are able to disproportionate

* To whom correspondence should be addressed. E-mail: Marie-Noëlle.Collomb@ujf-grenoble.fr (M.-N.C.); Alain.Deronzier@ujf-grenoble.fr (A.D.); jlatour@cea.fr (J.-M.L.). Fax: 33 4 76 51 42 67 (A.D.); 33 4 76 88 52 76 (J.-M.L.).

(1) (a) Departament de Quimica, Universitat de Girona. (b) Laboratoire d'Electrochimie Organique et de Photochimie Rédox, Université Joseph Fourier. (c) Laboratoire de Chimie Inorganique et Biologique, Université Joseph Fourier.

(2) Stadtman, E.; Berlett, P.; Chock, P. *Proc. Natl. Acad. Sci. U.S.A.* **1990**, *87*, 384.

(3) Halliwell, B.; Gutteridge, J. *Methods in Enzymology*; Academic Press: San Diego, CA, 1990.

10.1021/ic010721e CCC: $22.00
Published on Web 03/12/2002

H_2O_2 into more harmful dioxygen and water are an important part of this machinery.[4] A few of these enzymes possess a dinuclear manganese active site. They can exist in at least four different oxidation states, a reduced Mn^{II}_2 form, a mixed-valence $Mn^{II}Mn^{III}$ form, an oxidized Mn^{III}_2 form, and a superoxidized $Mn^{III}Mn^{IV}$ form.[4−7] However, it has been shown that the enzyme cycles exclusively between the Mn^{II}_2 and Mn^{III}_2 oxidation states during the catalysis and only these oxidation states are able to catalyze the dismutation of hydrogen peroxide at extremely high rates.[4−7] A recent X-ray structure diffraction at 1.6 Å resolution[8] shows that, in *Thermus thermophilus* catalase, the Mn···Mn separation is 3.18 Å in the reduced Mn^{II}_2 form and 3.14 Å in the oxidized Mn^{III}_2 form. Moreover, the two manganese ions are triply bridged by a $\mu_{1,3}$-carboxylate from a glutamate residue and two single atom bridges, the nature of which is not yet ascertained.[9] These bridges are believed to undergo changes during peroxide dismutation that are critical for catalysis, but their functional significance remains unknown.

In recent years, several kinds of dinuclear manganese model complexes have been reported showing catalase activity.[10−39] However, only a few of these functional model systems proceed via the $Mn^{II}-Mn^{II} \leftrightarrow Mn^{III}-Mn^{III}$ redox cycle similar to the enzyme. The first system, based on a series of dinuclear complexes of functionalized Schiff bases [Mn(2-OHsalpn)]$_2$,[17,18,28,30,31] is an excellent peroxide disproportionation catalyst in acetonitrile. The reaction can occur for over 5000 turnovers without an indication of catalyst decomposition. The second such model system employs a septadentate ligand with benzimidazolyl group and a single bridging alkoxide.[11,20,21,38,39] No catalyst decomposition is seen after 2000 turnovers. A third class of $Mn^{II}-Mn^{II}$ model complexes using a dicarboxylic acid as a bridge has been also reported as an efficient catalyst; however, no indication of their stability has been reported.[34,35]

In this context, as part of our synthetic explorations of complexes with the bpea tridentate ligand (bpea = *N*,*N*-bis-(2-pyridylmethyl)ethylamine),[40,41] we report here the facile synthesis, the crystal structure, and the main physical and chemical characterizations of a new tris(μ-acetato)dimanganese(II) complex, $[Mn^{II}_2(\mu\text{-}O_2CCH_3)_3(bpea)_2](PF_6)$ (**2**) which exhibits some interesting catalase-like activity. In the manganese(II) chemistry, only a few triply carboxylato bridged dimanganese(II) complexes have been previously synthesized,[42−47] but their redox properties and their reactivity have remained mostly unexplored.

We report also the crystal structure of the mononuclear manganese(II) complex, $[Mn^{II}(bpea)_2](PF_6)_2]$ (**1**), whose synthesis has been described in a previous work.[40] Moreover, the detailed study of the electrochemical behavior of these two complexes in organic medium (CH_3CN) is presented. On the basis of our previous electrochemical investigations[40,48−50] and those of Mukherjee et al.[51−53] on these kinds

(4) Khangulov, S. V.; Barynin, V. V.; Voevodskaya, N. V.; Grebenko, A. I. *Biochim. Biophys. Acta* **1990**, *1020*, 305.
(5) Penner-Hahn, J. E. In *Structural properties of the Mn site in the Mn catalases*; Pecoraro, V. L., Ed.; Verlag Chemie: New York, 1992; p 29.
(6) Dismukes, G. C. *Chem. Rev.* **1996**, *96*, 2909.
(7) Rüttinger, W.; Dismukes, G. C. *Chem. Rev.* **1997**, *97*, 1.
(8) Barynin, V. V.; Hempstead, P. D.; Vagin, A. A.; Antonyuk, S. V.; Melik-Adamyan, W. R.; Lamzin, V. S.; Harrison, P. M.; Artymiuk, P. J. *J. Inorg. Biochem.* **1997**, *67*, 196 and references therein.
(9) Antonyuk, S.; Melik-Adamyan, V.; Popov, A.; Lamzin, V.; Hempstead, P.; Harrison, P.; Artymyuk, P.; Barynin, V. *Crystallogr. Rep. (Transl. Kristallografiya)* **2000**, *45*, 105.
(10) Oishi, N.; Nishida, Y.; Kida, S. *Chem. Lett.* **1982**, 409.
(11) Mathur, P.; Crowder, M.; Dismukes, G. C. *J. Am. Chem. Soc.* **1987**, *109*, 5227.
(12) Stibany, R. T.; Gorun, S. M. *Angew. Chem., Int. Ed. Engl.* **1990**, *29*, 1156.
(13) Larson, E. J.; Pecoraro, V. L. *J. Am. Chem. Soc.* **1991**, *113*, 7809.
(14) Bossek, U.; Saher, M.; Weyhermüller, T.; Wieghardt, K. *J. Chem. Soc., Chem. Commun.* **1992**, 17801.
(15) Sakiyama, H.; Okawa, H.; Suzuki,.M..*J. Chem. Soc., Dalton Trans.* **1993**, 3823.
(16) Sakiyama, H.; Okawa, H.; Isobe, R. *J. Chem. Soc., Chem. Commun.* **1993**, 882.
(17) Gelasco, A.; Pecoraro, V. *J. Am. Chem. Soc.* **1993**, *115*, 7928.
(18) Pecoraro, V. L.; Baldwin, M. J.; Gelasco, A. *Chem. Rev.* **1994**, *94*, 807.
(19) Nishida, Y.; Akamatsu, T.; Tsuchiva, K.; Sakamoto, M. *Polyhedron* **1994**, *13*, 2251.
(20) Pessiki, P. J.; Khangulov, S. V.; Ho, D. M.; Dismukes, G. C. *J. Am. Chem. Soc.* **1994**, *116*, 891.
(21) Pessiki, P. J.; Dismukes, G. C. *J. Am. Chem. Soc.* **1994**, *116*, 898.
(22) Casey, M. T.; McCann, M.; Devereux, M.; Curran, M.; Cardin, C.; Convery, M.; Quillet, V.; Harding, C. *J. Chem. Soc., Chem. Commun.* **1994**, 2643.
(23) Devereux, M.; McCann, M.; Casey, M. T.; Curran, M.; Ferguson, G.; Cardin, C.; Convery, M.; Quillet, V. *J. Chem. Soc., Dalton Trans.* **1995**, 771.
(24) Nagata, T.; Mizukami, J. *J. Chem. Soc., Dalton Trans.* **1995**, 2825.
(25) Itoh, M.; Motoda, K.; Shindo, K.; Kamiusuki, T.; Sakiyama, H.; Matsumoto, N. Okawa, H. *J. Chem. Soc., Dalton Trans.* **1995**, 3635.
(26) Higuchi, C.; Sakiyama, H.; Okawa, H. Fenton, D. *J. Chem. Soc., Dalton Trans.* **1995**, 4015.
(27) Delroisse, M.; Rabion, A.; Chardac, F.; Tétard, D.; Verlhac, J. B.; Fraisse, L.; Séris, J. L. *J. Chem. Soc., Chem. Commun.* **1995**, 949.
(28) Gelasco, A.; Askenas, A.; Pecoraro, V. L. *Inorg. Chem.* **1996**, *35*, 1419.
(29) Aono, T.; Wada, H.; Yonemura, M.; Ohba, M.; Okawa, H.; Fenton, D. *J. Chem. Soc., Dalton Trans.* **1997**, 1527.
(30) Gelasco, A.; Kirk, M. L.; Kampf, J. W.; Pecoraro, V. L. *Inorg. Chem.* **1997**, *36*, 1829.
(31) Gelasco, A.; Bensiek, S.; Pecoraro, V. L. *Inorg. Chem.* **1998**, *37*, 3301.
(32) Mikuriya, M.; Fukumoto, H.; Kako, T. *Inorg. Chem. Commun.* **1998**, *1*, 225.
(33) Sasaki, Y.; Akamatsu, T.; Tsuchiya, K.; Ohba, S.; Sakamoto, M.; Nishida, Y. *Polyhedron* **1998**, *17*, 235.
(34) Xiang, D. F.; Tan, X. S.; Tang, W. X.; Xue, F.; Mak, T. C. W. *Polyhedron* **1998**, *17*, 1375.
(35) Xiang, D. F.; Duan, C. Y.; Tan, X. S.; Liu, Y. J.; Tang, W. X. *Polyhedron* **1998**, *17*, 2647.
(36) Nakamura, T.; Niwa, K.; Fujiwara, M.; Matsushita, T. *Chem. Lett.* **1999**, 1067.
(37) Palopoli, C.; Chansou, B.; Tuchagues, J.-P.; Signorella, S. *Inorg. Chem.* **2000**, *39*, 1458.
(38) Boelrijk, A. E. M.; Khangulov, S. V.; Dismukes, G. C. *Inorg. Chem.* **2000**, *39*, 3009.
(39) Boelrijk, A. E. M.; Dismukes, G. C. *Inorg. Chem.* **2000**, *39*, 3020.
(40) Collomb Dunand-Sauthier, M.-N.; Deronzier, A.; Romero, I. *J. Electroanal. Chem.* **1997**, *436*, 219.
(41) Romero, I.; Collomb, M.-N.; Llobet, A.; Perret, E.; Pécaut, J.; LePape, L.; Latour, J.-M. *Eur. J. Inorg. Chem.* **2001**, 69.
(42) Wieghardt, K.; Bossek, U.; Nuber, B.; Weiss, J.; Bonvoisin, J.; Corbella, M.; Vitols, S. E.; Girerd, J.-J. *J. Am. Chem. Soc.* **1988**, *110*, 7398.
(43) Matsushima, H.; Ishiwa, E.; Koikawa, M.; Nakashima, M.; Tokü, T. *Chem. Lett.* **1995**, 129.
(44) Osawa, M.; Singh, U. P.; Tanaka, M.; Moro-oka, Y.; Kitajima, N. *J. Chem. Soc., Chem. Commun.* **1993**, 310.
(45) Yamami, M.; Tanaka, M.; Sakiyama, H.; Koga, T.; Kobayashi, K.; Miyasaka, H.; Ohba, M.; Okawa, H. *J. Chem. Soc., Dalton Trans.* **1997**, 4595.
(46) Sinh, U. P.; Singh, R.; Hikichi, S.; Akita, M.; Moro-oka, Y. *Inor. Chim. Acta* **2000**, *301*, 273.
(47) Guidote, A. M., Jr.; Ando, K.; Kurusu, Y.; Nagao, H.; Masuyama, Y. *Inorg. Chim. Acta* **2001**, *314*, 27.

of complexes, we show here that the complexes $[Mn^{III}_2(\mu\text{-}O)(\mu\text{-}O_2CCH_3)_2(bpea)_2]^{2+}$ (**3**) and $[Mn^{IV}_2(\mu\text{-}O)_2(\mu\text{-}O_2CCH_3)(bpea)_2]^{3+}$ (**4**)[54−57] can be easily and selectively and quantitatively electrogenerated from **2** and from **1** in the presence of added $CH_3CO_2^-$ anions. Associated electrochemical backtransformations are also studied. In this article, we also investigated the catalytic activity toward the disproportionation of hydrogen peroxide of the binuclear complexes **2**, **3**, and the mixed-valence di-μ-oxo $[Mn^{III}Mn^{IV}(\mu\text{-}O)_2(\mu\text{-}O_2CCH_3)(bpea)_2]^{2+}$ (**5**) form. A reaction scheme will be proposed in light of their redox properties to explain the higher activity of **2**.

Experimental Section

Materials. Acetonitrile (CH_3CN, Rathburn, HPLC grade) was used as received and stored under an argon atmosphere in a glovebox. Tetra-*n*-butylammonium perchlorate (Bu_4NClO_4, Fluka) and hydrogen peroxide (70% in water, Aldrich) were used as received.

Ligand and Complexes. The ligand *N*,*N*-bis(2-pyridylmethyl)-ethylamine (bpea) was synthesized according to a method described previously.[54] The complexes $[Mn^{II}(bpea)_2](PF_6)_2$ (**1**), $[Mn^{III}Mn^{IV}(\mu\text{-}O)_2(\mu\text{-}O_2CCH_3)(bpea)_2](PF_6)_2$ (**5**), $[Mn^{IV}_2(\mu\text{-}O)_2(\mu\text{-}O_2CCH_3)(bpea)_2](BF_4)_3$ (**4**), and $[Mn^{III}_2(\mu\text{-}O)(\mu\text{-}O_2CCH_3)_2(bpea)_2](PF_6)_2$ (**3**) were prepared according to the literature.[40,54,56] For the synthesis of the binuclear complexes, PF_6^- or BF_4^- was employed as counterion instead of ClO_4^-.

$[Mn^{II}_2(\mu\text{-}O_2CCH_3)_3(bpea)_2](PF_6)$ (2). To a solution of bpea (0.102 g, 0.45 mmol) in methanol (5 mL) was added $Mn(O_2CCH_3)_2\cdot 4H_2O$ (0.109 g, 0.45 mmol), and after 15 min of stirring, sodium acetate (0.023 g, 0.27 mmol) was added. The resulting colorless solution was then stirred at room temperature for 30 min. After addition of KPF_6 (0.042 g, 0.23 mmol) the solution was evaporated and the residue dissolved in dichloromethane and filtered to remove some impurities. Addition of diethyl ether to the solution produced a white solid of **2** that was filtered out, washed with diethyl ether, and dried under vacuum. Yield: 0.160 g, 80%. Single crystals of **2** were grown by slow diffusion of diethyl ether in a concentrated solution of this complex in CH_2Cl_2. These crystals analyzed satisfactorily as $[Mn^{II}_2(\mu\text{-}O_2CCH_3)_3(bpea)_2](PF_6)$. Anal. Calcd for $C_{34}H_{43}F_6Mn_2N_6O_6P$ (886.59): C, 46.02; H, 4.85; N, 9.47. Found: C, 46.30; H, 5.06; N, 9.52. The formula for this complex was verified by fast bombardment atomic mass spectrometry (FAB), positive mode, *m*/*z* $[Mn_2(O_2CCH_3)_3(bpea)_2]^+ = 741$, and electrospray mass spectrometry (ESMS), *m*/*z* $[Mn_2(O_2CCH_3)_3(bpea)_2]^+ = 741$ and $[Mn_2(O_2CCH_3)_3(bpea)]^+ = 514$.

IR (KBr, cm^{-1}) (vs, very strong; s, strong; m, medium; w, weak; sh, shoulder): ν = 1619 (vs), 1603 (s), 1574 (m), 1483 (m), 1432 (vs), 1387 (m), 1365 (m), 1342 (w), 1310 (m), 1291 (m), 1268 (w), 1246 (w), 1224 (w), 1170 (w), 1156 (m), 1126 (m), 1103 (m), 1072 (w), 1047 (m), 1014 (s), 997 (w), 977 (w), 961 (w), 934 (w), 902 (m), 876 (m), 837 (vs), 762 (s), 741 (w), 729 (w), 646 (m), 614 (m), 557 (s), 505 (w), 472 (w), 416 (m).

Electronic spectral data in CH_3CN solution (λ_{max}, nm (ϵ, M^{-1} cm^{-1}): 257 (12 000).

Spectroscopies. Electronic absorption spectra were recorded on a Hewlett-Packard 8452A diode array spectrophotometer. Initial and electrolyzed solutions were transferred to a conventional cuvette cell in the glovebox. The cell was inserted into an optical translator connected to the spectrophotometer through a fiber optic system (Photonetics Spectrofip System). The optical fibers pass through the wall of the drybox via seals. Infrared spectra were recorded on a Perkin-Elmer Spectrum GX FTIR Spectrometer. X-Band EPR spectra were collected by using a Bruker spectrometer equipped with an Oxford Instrument cryostat ESR900. Fast atom bombardment mass spectra (FAB) were obtained on an AEI Kratos MS 50 spectrometer fitted with an Ion Tech Ltd.gu (Centre de Recherche sur les Macromolécules Végétales, Grenoble, France). Electrospray mass spectra (ES) were obtained on a LCQ Finnigan Thermoquest ESI source.

X-ray Structure Analysis. The data sets for the single-crystal X-ray studies were collected with Mo Kα radiation on a Brucker SMART diffractometer. All calculations were performed using the SHELXTL program.[58] The structure was solved by direct methods and refined by full-matrix least squares on F_2.

Magnetic Measurements. The magnetic susceptibility of compound **2** was measured over the remperature range 5−300 K at 0.5 and 5 T. The sample (35.01 mg) was contained in a Kel F bucket which had been independently calibrated. The data were corrected from diamagnetism using Pascal's constants.[59] The data have been simulated using the van Vleck equation derived from the Heisenberg exchange Hamiltonian ($H = -2JS_1S_2$):

$$\chi_m T = 0.75g^2\{[\exp(2k) + 5\exp(6k) + 14\exp(12k) + 30\exp(20k) + 55\exp(30k)]/[1 + 3\exp(2k) + 5\exp(6k) + 7\exp(12k) + 9\exp(20k) + 11\exp(30k)]\} + (TIP)T$$

Here $k = J/(0.695T)$. A strong correlation of g and TIP was observed which precludes the precise determination of either parameter. By contrast the exchange interaction J was estimated with a good precision 0.1 cm^{-1}. The goodness of fit R^2 amounted to 0.9998.

Electrochemistry. Electrochemical measurements were carried out using an EG&G PAR model 173 potentiostat equipped with a model 179 digital coulometer and a model 175 programmer with output recorded on a Sefram TGM 164 X−Y recorder. All electrochemical experiments were run under an argon atmosphere in a glovebox, using a standard three-electrode electrochemical cell. All potentials were referred to a Ag/Ag^+ (10 mM) reference electrode in acetonitrile + tetra-*n*-butylammonium perchlorate (TBAP) electrolyte. The potential of the regular ferrocene/ferrocenium (Fc/Fc^+) redox couple used as an internal standard was 0.07 V under our experimental conditions. The working electrodes were platinum disks polished with 1 μm diamond paste that were 5 mm in diameter for cyclic voltammetry (CV ; E_{pa}, anodic peak potential; E_{pc}, cathodic peak potential; $E_{1/2} = (E_{pa} + E_{pc})/2$; ΔE_p

(48) Collomb Dunand-Sauthier, M.-N.; Deronzier, A.; Pradon, X.; Ménage, S.; Philouze, C. *J. Am. Chem. Soc.* **1997**, *119*, 3173.
(49) Collomb Dunand-Sauthier, M.-N.; Deronzier, A.; Piron, A.; Pradon, X.; Ménage, S. *J. Am. Chem. Soc.* **1998**, *120*, 5373.
(50) Collomb Dunand-Sauthier, M.-N.; Deronzier, A.; Piron, A. *J. Electroanal. Chem*. **1999**, *463*, 119.
(51) Mahapatra, S.; Das, P.; Mukherjee, R. *J. Chem. Soc., Dalton Trans.* **1993**, 217.
(52) Mahapatra, S.; Lal. T. K.; Mukherjee, R. *Inorg. Chem.* **1994**, *33*, 1579.
(53) Lal, T. K.; Mukherjee, R. *Inorg. Chem.* **1998**, *37*, 2373.
(54) Pal, S.; Chan, M. K.; Armstrong, W. H. *J. Am. Chem. Soc.* **1992**, *114*, 6398.
(55) Pal, S.; Olmstead, M. M.; Armstrong, W. H. *Inorg. Chem.* **1995**, *34*, 4708.
(56) Mandal, S. K.; Armstrong, W. H. *Inorg. Chim. Acta* **1995**, *229*, 261.
(57) Mok, H. J.; Davis, J. A.; Pal, S.; Mandal, S. K.; Armstrong, W. H. *Inorg. Chim. Acta* **1997**, *263*, 385.
(58) Sheldrich, G. M. *SHELXTL, version 5.1, An Integrated System for Solving, Refining and Displaying Crystal Structures from Diffraction Data*; Siemens Analytical X-ray Instruments: Madison, WI, 1990.
(59) Kahn, O. *Molecular Magnetism*; VCH: New York, 1993.

$= E_{pa} - E_{pc}$) and 2 mm in diameter for rotating disk electrode experiments (RDE). Exhaustive electrolyses were carried out with a carbon felt electrode (RCV 2000, 65 mg cm^{-3}, from Le Carbone Lorraine).

Catalase-like Activity. In a typical experiment 2 mL of a 1 mM acetonitrile solution of complex was thermostated to 0 °C and 50 μL of a 9.91 M solution of hydrogen peroxide (250 equiv) was added. Dioxygen evolution was observed instantaneously and monitored volumetrically. Aliquots were taken after 20 s and transferred into an EPR tube or injected into an ESMS spectrometer.

Results

Syntheses. Complex **1** is synthesized, as described in our previous paper,[40] by the reaction of $Mn^{II}(PF_6)_2$ with bpea in an ethanol solution. To better characterize this complex, colorless monocrystals have been obtained by slow diffusion of diethyl ether in an ethanol solution of **1** and its structure has been determinated by X-ray crystallography.

On the other hand, the analogous reaction starting with $Mn^{II}(O_2CCH_3)_2 \cdot 4H_2O$ and $NaCH_3CO_2$ in ethanol solution yielded, after addition of KPF_6, a white precipitate of **2**. This complex was then recrystallized by slow diffusion of diethyl ether in a dichloromethane solution of **2** affording single crystals suitable for X-ray crystallography analysis. It must be noted that the synthesis of **1** requires the absence of acetate anions in the reaction mixture. Indeed, **2** is always the final product starting from $Mn^{II}(O_2CCH_3)_2 \cdot 4H_2O$ as manganese(II) salt, even in the presence of more than 2 equiv of bpea per Mn^{2+}. In contrary to the analogous dimanganese(II) $[Mn^{II}_2(\mu\text{-}O_2CCH_3)_3(L')_2](BPh_4)$ ($L' = N,N',N''$-trimethyl-1,4,7-triazacyclononane),[42] **1** and **2** are stable in the solid state as in organic solvents and not air sensitive. As for other complexes containing three acetato bridges,[42−47] the IR spectrum of **2** displays two prominent vibrations of the O−C−O portion of the μ-acetato group ν_{as} (1619 cm^{-1}) and ν_s (1432 cm^{-1}).

Description of the Crystal Structures. $[Mn^{II}(bpea)_2](PF_6)_2$ (1). Complex **1** crystallizes in the monoclinic space group $P2_1/n$ with four molecules per unit cell. Figure 1 shows two views of the ORTEP diagram together with the crystallographic numbering scheme for the cation $[Mn^{II}(bpea)_2]^{2+}$. The Mn atom is coordinated by six nitrogen atoms from two facially bound bpea ligands in a distorted octahedral fashion. Table 1 contains crystallographic data, and Table 2, selected bond distances and angles.

This complex shows disorder in the crystal structure manifested in the two possible positions that can occupy the two methylenic groups of one bpea ligand [C(21A)−(C(21B) and C(27A)−C(27B)] and aliphatic chains binding the amino nitrogens of the two bpea ligands [C(14A)−C(14B) and C(33A)−C(34A)−C(33B)−C(34B)] (Figure 1). These disorders lead to different bond distances and different bond angles between these exchanged atoms (Table 2).

The different electronic nature of the aliphatic and aromatic N-coordinating atoms of the bpea ligands induces geometrical distortions from the ideal octahedral geometry which are mainly manifested with the presence of significantly different Mn−N bond lengths. The two largest Mn−N bond distances

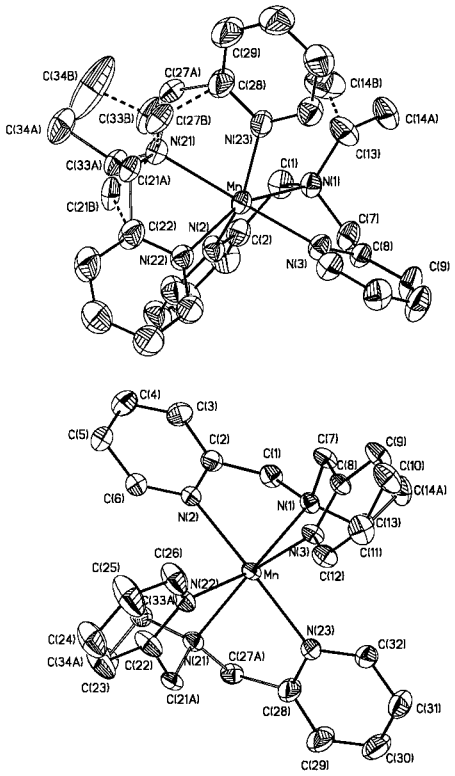

Figure 1. Two ORTEP views of the molecular structure of the cation of $[Mn^{II}(bpea)_2](PF_6)_2$ (**1**).

Table 1. Crystal Data and Details of the Refinement of the Crystal Structures of $[Mn^{II}(bpea)_2](PF_6)_2$ (**1**) and $[Mn^{II}_2(\mu\text{-}CH_3CO_2)_3(bpea)_2](PF_6)$ (**2**) with Standard Deviations in Parentheses

param	**1**	**2**
chem formula	$C_{28}H_{44}F_{12}MnN_6P_2$	$C_{34}H_{43}F_6Mn_2N_6O_6P$
fw	809.57	886.59
temp/K	298(2)	298(2)
λ/Å	0.710 73	0.710 73
cryst syst	monoclinic	orthorhombic
cryst size/mm × mm × mm	0.1 × 0.4 × 0.5	0.1 × 0.25 × 0.5
space group	$P2_1/n$	$C222_1$
a/Å	11.9288(7)	12.5686(16)
b/Å	22.5424(13)	14.4059(16)
c/Å	13.0773(7)	22.515(3)
α/deg	90	90
β/deg	100.5780	90
γ/deg	90	90
V/Å^3	3456.8(3)	4076.6(8)
Z	4	4
μ/mm^{-1}	0.570	0.735
no. of reflcns collcd	22 329	13 226
no. of indpdt reflcns	8395 ($R_{int} = 0.0470$)	4923 ($R_{int} = 0.0605$)
goodness-of-fit on F^2	0.859	0.930
final R indices [$I > 2\sigma(I)$]	$R_1 = 0.0461$	$R_1 = 0.0541$
	$wR_2 = 0.1101$	$wR_2 = 0.1341$
R indices (all data)	$R_1 = 0.1222$	$R_1 = 0.1078$
	$wR_2 = 0.1255$	$wR_2 = 0.1499$
largest diff peak, hole/e Å^{-3}	0.377, −0.294	0.819, −0.222

correspond to the Mn−N aliphatic bonds (Mn−N(1), 2.3498 (19) Å; Mn−N(21), 2.311(2) Å), while the four shortest correspond to the Mn−N aromatic bonds (Mn−N(3), 2.231-(2) Å; Mn−N(2), 2.280(2) Å; Mn−N(22), 2.282(2) Å; Mn−N(23), 2.262(2) Å). The same tendency has been observed in other similar manganese complexes with the same ligand.[41,54−57] The spatially constrained nature of the tridentate facial bpea ligand also produces geometrical distortions

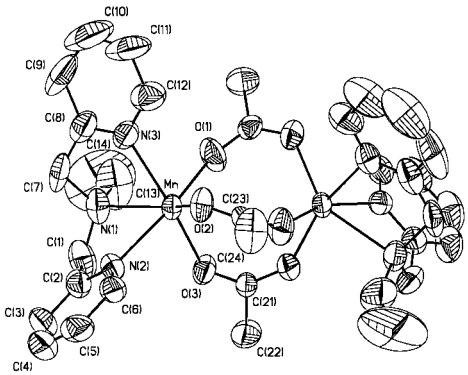

Figure 2. ORTEP view of the molecular structure of the cation of $[Mn_2^{II,II}(\mu\text{-}CH_3CO_2)_3(bpea)_2](PF_6)$ (**2**).

Table 2. Selected Bond Lengths (Å) and Bond Angles (deg) for **1**

Mn−N(3)	2.231(2)	N(21)−C(21A)	1.472(4)
Mn−N(23)	2.262(2)	N(21)−C(27A)	1.475(4)
Mn−N(2)	2.280(2)	N(21)−C(27B)	1.549(9)
Mn−N(22)	2.282(2)	N(21)−C(33A)	1.504(4)
Mn−N(21)	2.311(2)	C(21A)−C(22)	1.538(5)
Mn−N(1)	2.3498(19)	C(21B)−C(22)	1.633(9)
C(13)−C(14B)	1.209(12)	C(27A)−C(28)	1.560(5)
C(13)−C(14A)	1.476(5)	C(27B)−C(28)	1.690(11)
N(21)−C(33B)	1.435(10)	C(33A)−C(34A)	1.541(8)
N(21)−C(21B)	1.456(9)	C(33B)−C(34B)	1.51(2)
N(3)−Mn−N(23)	92.17(8)	N(22)−Mn−N(1)	155.42(8)
N(3)−Mn−N(2)	106.38(8)	N(21)−Mn−N(1)	123.10(7)
N(23)−Mn−N(2)	153.85(9)	C(7)−N(1)−C(1)	109.1(2)
N(3)−Mn−N(22)	92.91(8)	C(14B)−C(13)−N(1)	125.4(7)
N(23)−Mn−N(22)	106.29(9)	C(14A)−C(13)−N(1)	119.6(3)
N(2)−Mn−N(22)	91.31(8)	C(21B)−N(21)−C(27A)	145.5(4)
N(3)−Mn−N(21)	157.54(7)	C(21A)−N(21)−C(27A)	110.5(3)
N(23)−Mn−N(21)	73.89(8)	N(21)−C(21A)−C(22)	109.3(3)
N(2)−Mn−N(21)	92.90(7)	N(21)−C(21B)−C(22)	105.1(5)
N(22)−Mn−N(21)	74.87(8)	N(21)−C(27A)−C(28)	107.3(3)
N(3)−Mn−N(1)	74.87(7)	N(21)−C(27B)−C(28)	97.9(5)
N(23)−Mn−N(1)	95.59(8)	N(21)−C(33A)−C(34A)	116.1(4)
N(2)−Mn−N(1)	72.47(7)	N(21)−C(33B)−C(34B)	115.3(11)

from the ideal octahedron which are chiefly manifested in the N−Mn−N bond angles. Thus, the N−Mn−N bond angles with N atoms belonging to the same bpea are about 17° below 90° (ranging from 72.47 to 74.87°) between N aromatic and N aliphatic and 17° above 90° between N aromatics. The amino nitrogens are coordinated in a cis fashion (N(1)−Mn−N(21) bond angle of 123.10(7)°). The structure of **1** is very similar to that of its bis(picolylamine) (bpa) analogue.[60] While both ligands can adopt meridional[55] or several types of facial[54−57] coordinations, it is noteworthy that in both complexes they wrap around the Mn atom in the same way providing a pyridine nitrogen in a trans position to an aliphatic nitrogen. The only difference between the two complexes resides in slightly shorter Mn−N distances in the bpa complexes in line with its slightly smaller electron-donating properties.

$[Mn^{II}_2(\mu\text{-}O_2CCH_3)_3(bpea)_2](PF_6)$ (2). Figure 2 shows the cation $[Mn^{II}_2(\mu\text{-}O_2CCH_3)_3(bpea)_2]^+$ and the atom labeling scheme. Table 1 summarizes the crystallographic data, and Table 3, important bond lengths and angles. Each manganese atom is bound by three nitrogen atoms from a facially

(60) Glerup, J.; Goodson, P. A.; Hodgson, D. J.; Michelsen, K.; Nielsen, K. M.; Weibe, H. *Inorg. Chem.* **1992**, *31*, 4611.

Table 3. Selected Bond Lengths (Å) and Bond Angles (deg) for **2**

Mn(1)−Mn	3.915	Mn−N(3)	2.292(5)
Mn−O(1)	2.106(3)	Mn−N(2)	2.314(4)
Mn−O(2)	2.110(3)	Mn−N(1)	2.406(4)
Mn−O(3)	2.128(3)		
O(1)−Mn−O(2)	108.64(16)	O(3)−Mn−N(2)	84.42(14)
O(1)−Mn−O(3)	90.65(17)	N(3)−Mn−N(2)	98.01(15)
O(2)−Mn−O(3)	109.56(14)	O(1)−Mn−N(1)	93.09(16)
O(1)−Mn−N(3)	82.06(16)	O(2)−Mn−N(1)	148.99(13)
O(2)−Mn−N(3)	87.73(17)	O(3)−Mn−N(1)	91.51(16)
O(3)−Mn−N(3)	162.65(16)	N(3)−Mn−N(1)	73.29(19)
O(1)−Mn−N(2)	163.07(16)	N(2)−Mn−N(1)	70.93(15)
O(2)−Mn−N(2)	88.25(14)		

coordinated bpea ligand and three bridging acetates in a strongly distorded octahedral fashion. This complex adopts a symmetric structure. The two manganese atoms are equivalent since the complex has a C_2 symmetry axis passing through the C(21) and C(22) atoms of the O(3)−C(21) acetate bridge. The three acetates are in the familiar bidentate $\mu_{1,3}$ syn−syn bridging mode. The facial mode of coordination of the bpea ligands to the metal center is dictated by the orientation of these bridging ligands. This coordination produces geometrical distortions from the ideal octahedron which are manifested in the N−Mn−N bond angles (N(3)−Mn−N(2), 98.01(15)°; N(3)−Mn−N(1), 73.29(19)°; N(2)−Mn−N(1), 70.93(15)°) and also between two oxygen atoms of two acetates (O(1)−Mn−O(2), 108.64(16)°; O(2)−Mn−O(3), 109.56(14)°). The same tendency has been observed for the analogous dimanganese(II) complex $[Mn^{II}_2(\mu\text{-}O_2CCH_3)_3(L')_2](BPh_4)$.[42] The Mn−Mn distance of 3.915 Å compares well with those observed in two other tris($\mu_{1,3}$-carboxylate)-bridged complexes $[Mn^{II}_2(\mu\text{-}O_2CCH_3)_3(L')_2](BPh_4)$ (4.034 Å)[42] and $[(Tp^{iPr_2})Mn^{II}(\mu\text{-}O_2CC_6H_5)_3Mn^{II}(Tp^{iPr_2}H)]$ (Tp^{iPr_2} = hydrotris(3,5-diisopropyl-1-pyrazolyl)borate) (4.006 Å).[46] On the other hand, it is longer than that of the third $\mu_{1,3}$ complex $[Mn^{II}_2(\mu\text{-}O_2CC(CH_3)(C_6H_5)_2)_3(bpy)_2](PF_6)$ (bpy = 2,2′-bipyridine) (3.688 Å).[43] The Mn−O distances of 2.106(3), 2.110(3), and 2.128(3) Å for the acetato bridges are consistent with the values observed in the manganese complexes adopting the same $\mu_{1,3}$ mode for the carboxylate bridges (2.00−2.24 Å).[42,43,46] Moreover, as observed for **1,** the Mn−N bonds distances of the bpea ligand are different. The largest one corresponds to the Mn−N aliphatic bond (Mn−N(1), 2.406(4) Å), while the two shortest correspond to the Mn−N aromatic bonds (Mn−N(2), 2.314(4); Mn−N(3), 2.292(5) Å).

Magnetic Properties of 2. The magnetic susceptibility of **2** has been investigated in the temperature range 5−300 K at 0.5 and 5 T. Figure 3 illustrates the temperature dependence of the product of the molar magnetic susceptibility (χ_m) by temperature. The room-temperature value of $\chi_m T$ is ca. 8.75 $cm^3 \cdot K \cdot mol^{-1}$ as expected for two noninteracting spins $S = 5/2$. When T decreases $\chi_m T$ decreases smoothly until 70 K, where it reaches ca. 7.5 $cm^3 \cdot K \cdot mol^{-1}$ and then more abruptly to ca. 1.2 $cm^3 \cdot K \cdot mol^{-1}$ at 5 K. Such a behavior is characteristic of a pair of weakly antiferromagnetically coupled manganese(II) ions. It is noteworthy that the χ_m vs T curve exhibits a maximum at ca. 10 K (data not shown). The experimental data could be accounted for by using the

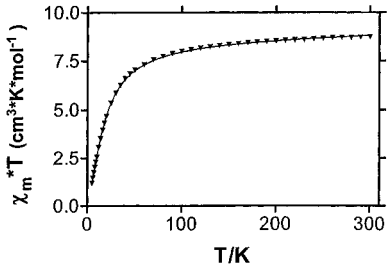

Figure 3. Temperature dependence of $\chi_m T$ for **2** (▼, experimental data obtained at 0.5 T; ---, calculated values ; see text).

Van Vleck equation for two interacting spins 5/2 (see Experimental Section). The solid line in Figure 3 represents the best fit obtained with the following parameters $g = 2.03$, $J = -1.3$ cm^{-1}, and TIP $= 1 \times 10^{-4}$ cm^3·mol^{-1}.

Electrochemistry. As we will see, oxidation of **2** in CH_3CN is a fully irreversible process leading first to the mono(μ-oxo) complex **3**, which can be further oxidized into the bis(μ-oxo) one **4**. So we have first reinvestigated in detail the electrochemical behavior of the complex **3**, especially the influence of the sweep rate on the CV, in view to identify the transient species.

Electrochemical Properties of 3. The shape of the cyclic voltammogram of a solution of **3** depends on the potential scan rate. At a high sweep rate ($v = 500$ mV s^{-1}, Figure 4A), three quasi-reversible waves appear at $E_{1/2}{}^{3A} = 0.76$ V ($E_{pa}{}^{3A} = 0.83$ V and $E_{pc}{}^{3A} = 0.7$ V; $\Delta E_p = 130$ mV), $E_{1/2}{}^{3B} = 1.37$ V ($E_{pa}{}^{3B} = 1.4$ V and $E_{pc}{}^{3B} = 1.34$ V; $\Delta E_p = 70$ mV), and $E_{1/2}{}^{3C} = -0.35$ V ($E_{pa}{}^{3C} = -0.32$ V and $E_{pa}{}^{3C} = -0.38$ V; $\Delta E_p = 60$ mV). The two oxidation waves are respectively attributed to the (III,III)/(III,IV) and (III,IV)/(IV,IV) redox couples (eqs 1 and 2)

$$[Mn^{III}{}_2(O)(O_2CCH_3)_2(bpea)_2]^{2+} \overset{E}{\rightleftarrows} [Mn^{III}Mn^{IV}(O)(O_2CCH_3)_2(bpea)_2]^{3+} + e^- \quad (1)$$

$$[Mn^{III}Mn^{IV}(O)(O_2CCH_3)_2(bpea)_2]^{3+} \rightleftarrows [Mn^{IV}{}_2(O)(O_2CCH_3)_2(bpea)_2]^{4+} + e^- \quad (2)$$

and the reduction wave to the (III,III)/(III,II) one:

$$[Mn^{III}{}_2(O)(O_2CCH_3)_2(bpea)_2]^{2+} + e^- \rightleftarrows [Mn^{III}Mn^{II}(O)(O_2CCH_3)_2(bpea)_2]^{+} \quad (3)$$

The electrogenerated oxidized $[Mn^{III}Mn^{IV}(\mu\text{-}O)(\mu\text{-}O_2CCH_3)_2(bpea)_2]^{3+}$ and $[Mn^{IV}{}_2(\mu\text{-}O)(\mu\text{-}O_2CCH_3)_2(bpea)_2]^{4+}$ and the reduced $[Mn^{III}Mn^{II}(\mu\text{-}O)(\mu\text{-}O_2CCH_3)_2(bpea)_2]^{+}$ species are not stable at the time scale of controlled potential electrolyses. The instability of these species is clearly observed during the recording of cyclic voltammograms of **3** at moderate or low scan rate ($v = 200$ and 10 mV s^{-1}, respectively) (Figure 4B,C). It then appears that the slower the scan rate, the more irreversible the three wave systems.

As described previously,[40] the first oxidation peak at $E_{pa}{}^{3A} = 0.83$ V involves an electrochemical chemical electrochemical (ECE) mechanism leading to the formation of the bis(μ-oxo) $[Mn^{IV}{}_2(\mu\text{-}O)_2(\mu\text{-}O_2CCH_3)(bpea)_2]^{3+}$ (**4**) complex

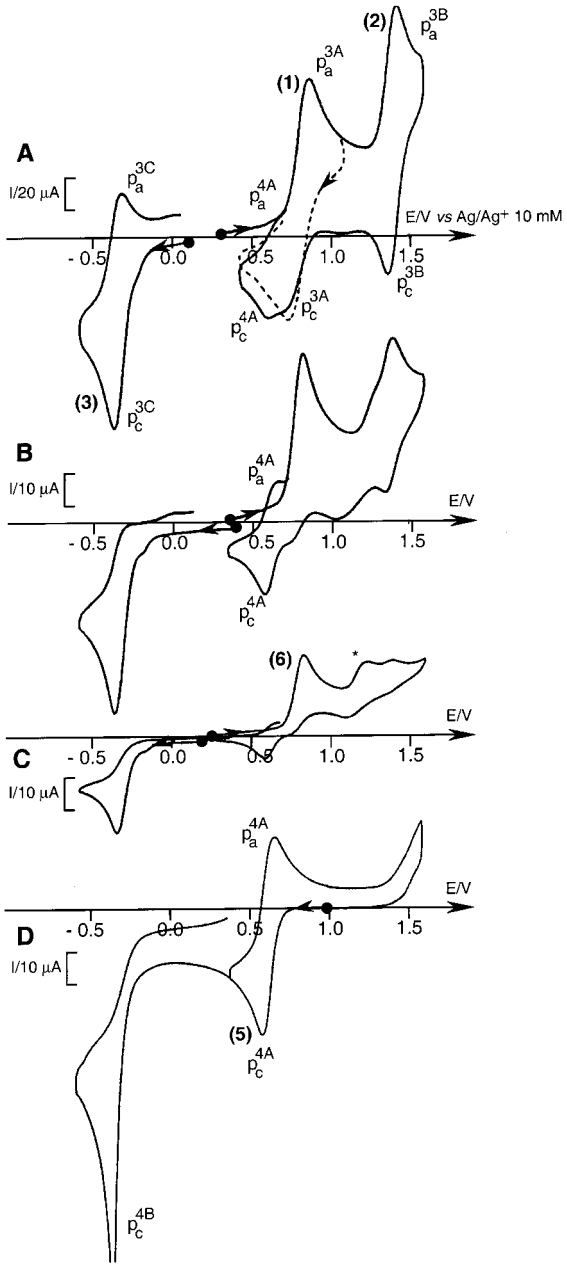

Figure 4. Cyclic voltammograms at a Pt electrode (diameter 5 mm) in CH_3CN + 0.1 M TBAP of (A) 1 mM $[Mn^{III}{}_2(\mu\text{-}O)(\mu\text{-}CH_3CO_2)_2(bpea)_2](PF_6)_2$ (**3**), sweep rate $v = 500$ mV s^{-1}, (B) $v = 100$ mV s^{-1}, (C) $v = 10$ mV s^{-1}, and (D) after exhaustive oxidation at 0.90 V with $v = 100$ mV s^{-1}.

(eqs 1, 4, and 5). Indeed, the one-electron-oxidized form of **3**, $[Mn^{III}Mn^{IV}(\mu\text{-}O)(\mu\text{-}O_2CCH_3)_2(bpea)_2]^{3+}$, is moderaly stable as shown by the weak intensity of its corresponding reduction peak at $E_{pc}{}^{3A} = 0.70$ V at moderate or low scan rate (Figure 4B,C) and reacts with residual water of the solvent to form the binuclear $[Mn^{III}Mn^{IV}(\mu\text{-}O)_2(\mu\text{-}O_2CCH_3)(bpea)_2]^{3+}$ complex **5** by substitution of an acetate bridge by an oxo one:

$$[Mn^{III}Mn^{IV}(O)(O_2CCH_3)_2(bpea)_2]^{3+} + H_2O \xrightarrow{C} [Mn^{III}Mn^{IV}(O)_2(O_2CCH_3)(bpea)_2]^{2+} + CH_3CO_2{}^- + 2H^+ \quad (4)$$

This latter complex is oxidized to its (IV,IV) form **4** at the

potential of the oxidation of the initial complex **3**, as a consequence of its easier oxidation:

$$[Mn^{III}Mn^{IV}(O)_2(O_2CCH_3)(bpea)_2]^{2+} \underset{b}{\overset{E\ a}{\rightleftarrows}} [Mn^{IV}{}_2(O)_2(O_2CCH_3)(bpea)_2]^{3+} + e^- \quad (5)$$

Equation 6a summarizes the overall reaction:

$$[Mn^{III}{}_2(O)(O_2CCH_3)_2(bpea)_2]^{2+} + H_2O \overset{a}{\rightleftarrows} [Mn^{IV}{}_2(O)_2(O_2CCH_3)(bpea)_2]^{3+} + CH_3CO_2{}^- + 2H^+ + 2e^- \quad (6)$$

The formation of **4** on the time scale of the cyclic voltammogram is indicated on the reverse scan and on the following positive scan (Figure 4A−C) by the appearance of a reversible redox system located at $E_{1/2}{}^{4A} = 0.61$ V, typical of its one-electron reduction. It must be noted that an additional quasi-reversible wave appears at lower scan rates which is clearly visible at 10 mV s^{-1} at a potential of 1.21 V (denoted by an asterisk in Figure 4C) located between the two oxidation waves of the **3** and **5** species. This system corresponds probably to an intermediate species produced during the chemical transformation of $[Mn^{III}Mn^{IV}(\mu\text{-}O)(\mu\text{-}O_2CCH_3)_2(bpea)_2]^{3+}$ into **5**.

As previously shown,[40] **4** can be generated with a 95% yield after an exhaustive oxidation at 0.9 V of a solution of **3** (eq 6) after 2 electrons/complex have been consumed. The amount of electrogenerated **4** is estimated from the absorption spectrum of the resulting brown solution at 454 nm using the ϵ value of 2180 mol^{-1} cm^{-1}.[55] The cyclic voltammogram obtained at 100 mV s^{-1} is typical of the electroactivity of **4** (Figure 4D) with a reversible one-electron reduction wave at $E_{1/2}{}^{4A} = 0.61$ V ($E_{pa}{}^{4A} = 0.64$ V and $E_{pc}{}^{4A} = 0.58$ V; $\Delta E_p = 60$ mV) (couple (IV,IV)/(III,IV)) (eq 5) followed by another irreversible one at $E_{pc}{}^{4B} = -0.44$ V corresponding to the irreversible reduction of **5**. In a solution containing a chemically prepared sample of **4**, this latter peak appears as a quasi-reversible wave at $E_{1/2}{}^4 = -0.29$ V ($\Delta E_p = 80$ mV).[40,55] For the electrogenerated sample of **4**, the irreversibility of this wave is due to the superimposition at this potential of the irreversible reduction of the free protons released since the formation of **4** (eq 6) involves the release of 2 protons and 1 mol of $CH_3CO_2{}^-$/mol of **3**. The reduced green form (III,IV) **5**[55] (eq 5b) of **4** can only be obtained in a ca. 75% yield after a subsequent controlled potential reduction at 0.4 V of the solution (consumption of 1.1 electrons/molecule of **3**). Beside this III,IV species, **3** is reformed in a ca. 25% yield.[40]

Electrochemical Behavior of 2. The CV of a solution of **2** in CH_3CN displays first an irreversible oxidation peak at $E_{pa}{}^2 = 0.44$ V at $\upsilon = 100$ mV s^{-1} corresponding to the oxidation of the metal centers of the complex (Figure 5A). It is worth noting that a similar CV is obtained if **2** is formed in situ by direct mixing of Mn^{2+} cations, bpea ligand, and $CH_3CO_2{}^-$ in a 1:1:3 stoichiometry in CH_3CN. The oxidation peak $E_{pa}{}^2$ is followed by a series of peak systems very close to those of the Figure 3B showing that oxidation of **2** leads to **3**. This electroinduced transformation is faster than the corresponding oxidation of **3** into **4**. Indeed, the oxidation peak $E_{pa}{}^2$ on the CV of **2** appears fully irreversible even at a sweep rate of $\upsilon = 500$ mV s^{-1}.

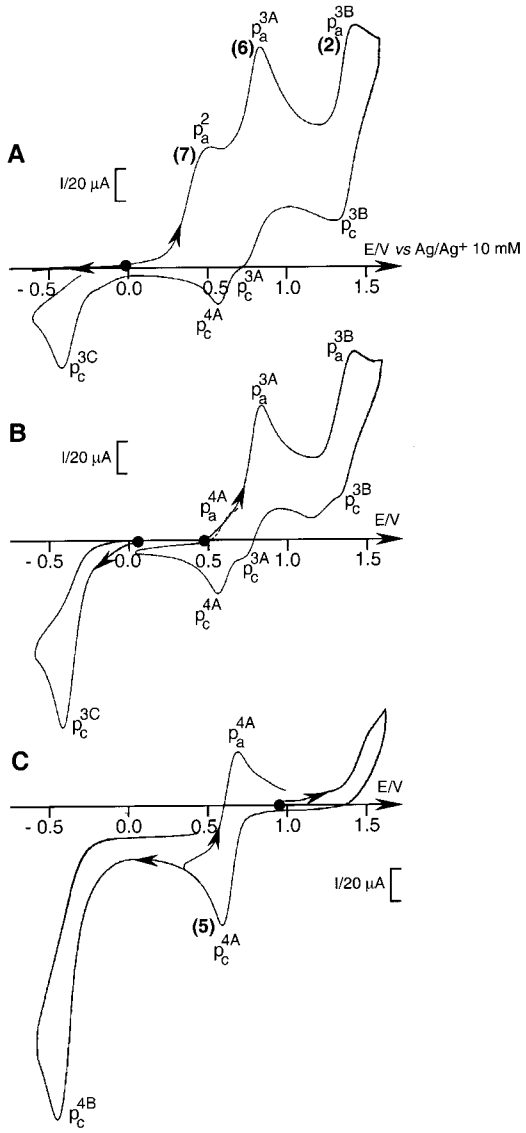

Figure 5. Cyclic voltammograms at a Pt electrode (diameter 5 mm) in CH_3CN + 0.1 M TBAP of (A) 1 mM $[Mn^{II}{}_2(\mu\text{-}CH_3CO_2)_3(bpea)_2](PF_6)$ (**2**)-**2,** (B) solution A after exhaustive oxidation at 0.60 V, and (C) solution B after exhaustive oxidation at 0.90 V with sweep rate $\upsilon = 100$ mV s^{-1}.

The formation of **3** on the time scale of the CV is clearly evidenced by the presence of its typical partially reversible oxidation waves at $E_{1/2}{}^{3A} = 0.76$ V and $E_{1/2}{}^{3B} = 1.37$ V at $\upsilon = 100$ mV s^{-1} and by its irreversible reduction peak at $E_{pc}{}^{3C} = -0.32$ V (Figure 5A). Complex **4**, formed by oxidation of **3** at $E_{pa}{}^{3A} = 0.83$ V, is also detected on the cyclic voltammogram by its first reduction peak at $E_{pc}{}^{4A} = 0.58$ V. As expected, a controlled potential oxidation of a solution of **2** conducted at 0.60 V consumes 2 electrons/binuclear **2** complex and furnishes mainly **3** (yield: 80%). The cyclic voltammogram of the resulting solution exhibits the typical electroactivity of **3** (Figure 5B) at 100 mV s^{-1}. Complex **3** containing the $\{Mn^{III}{}_2(\mu\text{-}O)(\mu\text{-}O_2CCH_3)_2\}^{2+}$ core is formed as the result of the metal oxidation of **2**. The proposed

Scheme 1

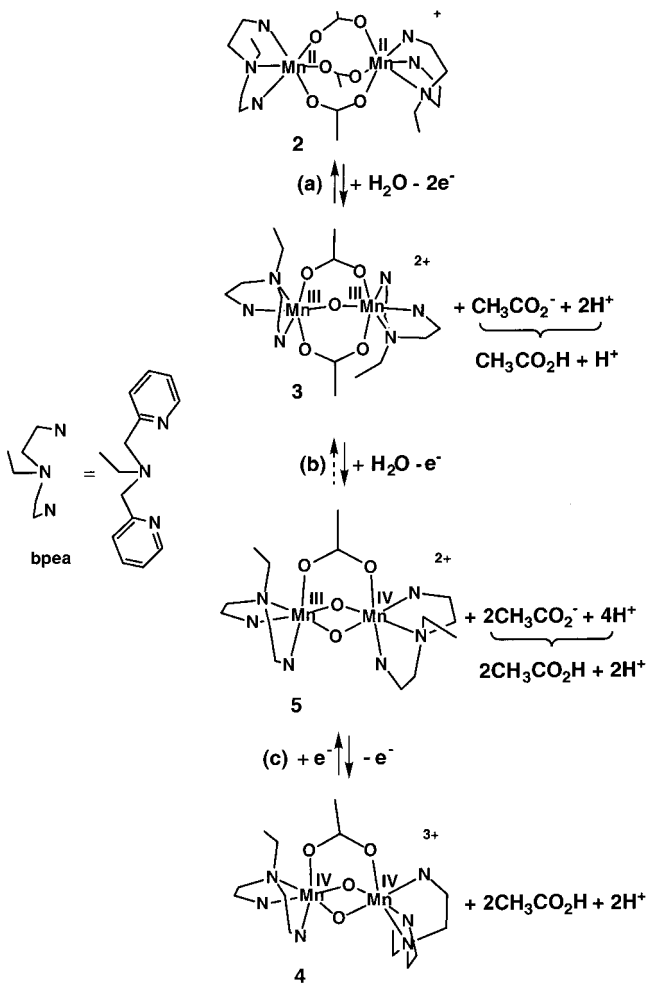

process involved in the oxidation of **2** is summarized in eq 7a (Scheme 1a).

$$[Mn^{II}_2(O_2CCH_3)_3(bpea)_2]^+ + H_2O \underset{b}{\overset{a}{\rightleftharpoons}} [Mn^{III}_2(O)(O_2CCH_3)_2(bpea)_2]^{2+} + CH_3CO_2^- + 2H^+ + 2e^- \quad (7)$$

The oxidation of **2** into **3** involves the formation of an oxo bridge between the two manganese ions, by deprotonation of water in the solvent and the release of one acetate anion. We can assume that the released acetate anions are probably protonated by the electrogenerated protons. The amount of **3** is estimated by the height of the electrochemical waves and by its visible absorption band at 488 nm using the ϵ value of 517 L mol^{-1} cm^{-1}, compared to a chemically prepared sample of **3**.[56]

A further controlled potential oxidation at 0.9 V results in the formation of **4** (yield 96%) after the consumption of 2 additional electrons/mol of initial **2** (eq 6a) (Scheme 1b,c). The cyclic voltammogram of the brown solution obtained (Figure 5C), as well as its visible absorption spectrum, is characteristic of a solution of **4**.

It must be noted that **4** can be generated directly with a 96% yield by a 4 electron oxidation of **2** at 0.90 V (eq 8a, summation of eqs 6 and 7) (Scheme 1a−c).

$$[Mn^{II}_2(O_2CCH_3)_3(bpea)_2]^+ + 2H_2O \underset{b}{\overset{a}{\rightleftharpoons}} [Mn^{IV}_2(O)_2(O_2CCH_3)(bpea)_2]^{3+} + 2CH_3CO_2^- + 4H^+ + 4e^- \quad (8)$$

On the other hand, the reaction 7 is an overall reversible process. A subsequent controlled potential reduction at −0.6 V of the electrochemically generated solution of **3** restores entirely the initial amount of **2** after the consumption of 2 electrons/molecule of **3**. Likewise, the initial amount of **2** (Scheme 1a) is entirely obtained by a controlled potential reduction at −0.6 V of the electrochemically generated solution of **4** (reaction 8b) (Scheme 1a−c) after consumption of 3.8 electrons/molecule of **4**.

Electrochemical Properties of 1. As we have previously reported,[40] the cyclic voltamogramm of **1** chemically prepared or formed in situ from a simple mixing of Mn^{2+} cations and 2 molar equiv of bpea (Scheme S1) in CH_3CN + 0.1 M TBAP shows a shoulder around 0.9 V assigned to the metal oxidation process followed by an ill-defined anodic peak corresponding to the pyridine oxidation of the ligand bpea (Figure 6A). No clear reduction peaks are detected on the reverse scan, which should attest the formation of a binuclear species.

We found that a clean dimerization reaction by electrochemical oxidation of **1** and thus the selective and sequential formation of the binuclear complexes $[Mn^{III}_2(\mu\text{-}O)(\mu\text{-}O_2CCH_3)_2(bpea)_2]^{2+}$ (**3**) and $[Mn^{IV}_2(\mu\text{-}O)_2(\mu\text{-}O_2CCH_3)(bpea)_2]^{3+}$ (**4**) takes place in the presence of added acetate anions. Indeed, the addition of 3 molar equiv of acetate/**1** (as Bu_4N^+ salt) in solution induces a drastic change of the cyclic voltammogram (Figure 6B). Isolation of **2** allows us now to attribute this change to the in-situ formation of this complex by release of 1 bpea ligand/manganese and formation of three acetate bridges following eq 9 (Scheme S1).

$$2[Mn^{II}(bpea)_2]^{2+} + 3CH_3CO_2^- \rightarrow [Mn^{II}_2(O_2CCH_3)_3(bpea)_2]^+ + 2bpea \quad (9)$$

The CV of the resulting solution is similar to that of a solution of **2** containing 2 molar equiv of added free bpea. Indeed, the irreversible oxidation peak located at E_{pa}^{1A} = 0.68 V is typical of the oxidation of the tertiary amine group of the free bpea, and those located at E_{pa}^{1B} = 1.26 V and E_{pa}^{1C} = 1.48 V are similar to the oxidation of the two pyridines (Figure 6B). The irreversible metal-based two-electron oxidation peak in **2** is shifted to a less positive value of E_{pa}^{2B} = 0.44 V compared to **1** and is associated with the formation of **3** (eq 6). This is proven by the presence on the cyclic voltammogram of the additional oxidation peak at E_{pa}^{3A} = 0.83 V involving the generation of the complex **4**.

The quantitative formation of **3** is obtained by an oxidation of the solution at 0.5 V (eq 7). A further controlled potential oxidation at 1.0 V results in the quantitative formation of **4** (eq 6) after the consumption of a second 1 electron/mol of initial **1** (Scheme S1), while a subsequent reduction at −0.6 V restores quantitatively the initial solution containing **2** and

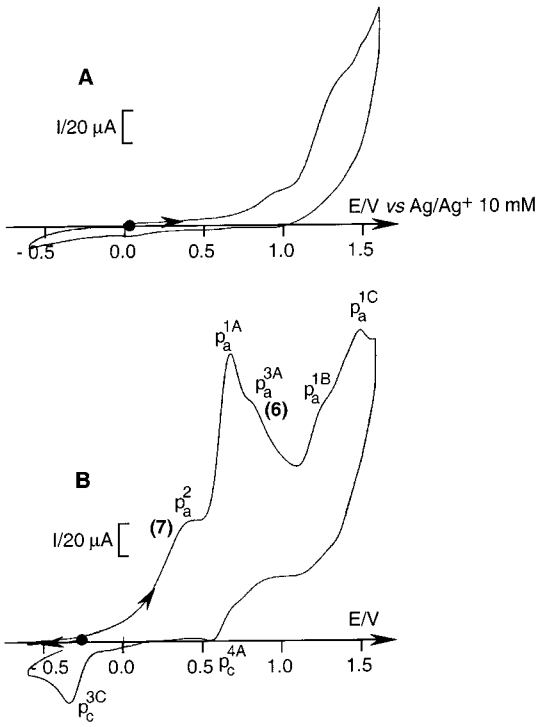

Figure 6. Cyclic voltammograms at a Pt electrode (diameter 5 mm) in CH_3CN + 0.1 M TBAP of (A) 1 mM $[Mn^{II}(bpea)_2](PF_6)_2$ (**1**) and (B) after addition of 3 mM of $CH_3CO_2^-$ anions as Bu_4N^+ salt with sweep rate υ = 100 mV s^{-1}.

2 molar equiv of free bpea (eq 8b). These results shows that all the redox reactions are chemically reversible.[40]

It is noteworthy that, during the oxidations of **2** into **3** and then of **3** into **4**, the electrogenerated protons (Scheme S1) protonate partially the free bpea ligands instead of the acetate anions, since on the resulting cyclic voltammograms (not shown), the additional peaks at $E_{pa}^{1A} = 0.68$ V and then at $E_{pa}^{1B} = 1.26$ V disappear.

Catalase-like Activity. 2, **3**, and their dimanganese(III,-IV) analogue **5** were studied for their ability to disproportionate hydrogen peroxide. When H_2O_2 is added to a solution of **2**, the colorless solution turns yellow-orange. The same but more intense color is obtained when H_2O_2 is added to an orange-red solution of **3** or to a green solution of **5**. In every case, the color is bleached at the end of the reaction pointing to the formation of Mn^{II} species. Figure 7 illustrates the time dependence of dioxygen evolution for the three complexes. **3** and **5** exhibit identical activities within experimental error (rate of O_2 production: **3**, 0.7(1) mL of O_2 min^{-1}; **5**, 0.75(10) mL of O_2 min^{-1}) (Figure 7A) and disproportionate 100% of added H_2O_2 in about 90 min. **2** is far more active since it disproportionates H_2O_2 quantitatively in ca. 10 min (**2**, 1.8(1) mL of O_2 min^{-1}). This difference roughly corresponds to a factor of 2.5 in their respective initial rates. However, when a second addition of H_2O_2 is made at the end of the reaction of **2**, the rate of dioxygen evolution is close to that of **3** and **5** (0.6(1) mL of O_2 mL^{-1}) (Figure 7A). Figure 7B illustrates the effect of acetate addition, 1 or 5 equiv, on the kinetics of dioxygen evolution: it is clear that excess acetate inhibits the disproportionation reaction and that this effect increases with acetate

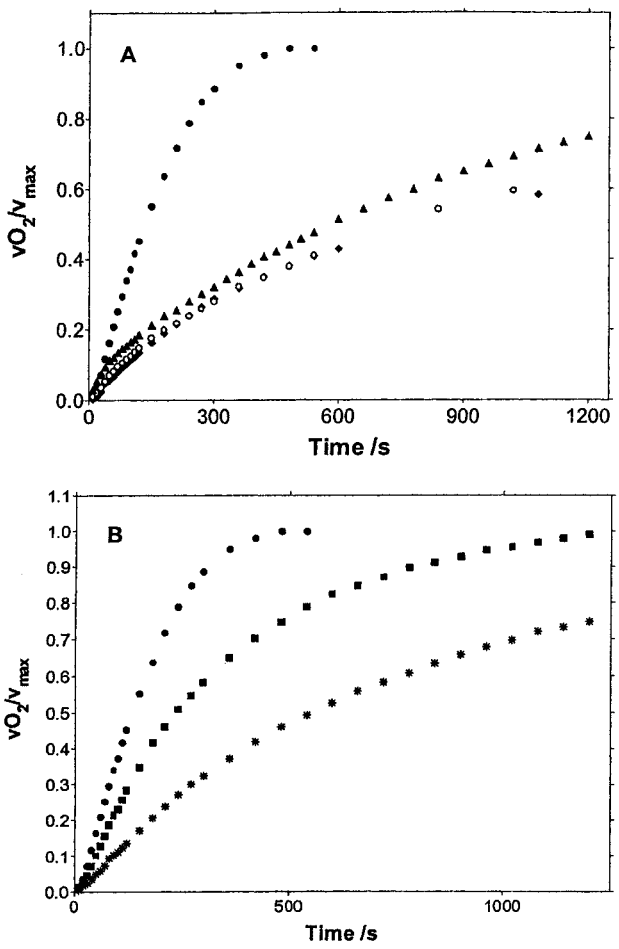

Figure 7. Time dependence of the dioxygen evolution catalyzed by **3** (○), **5** (▲), and **2** (first addition ●; second addition ◆; in the presence of $(NBu_4)(OAc)$ 1 equiv, ■♀ and 5 equiv, *). Conditions: [complex] = 1 mM in CH_3CN; $[H_2O_2]$ = 250 mM; T = 273 K.

concentration (in the presence of 1 equiv of $NaOAc_2$, 0.9(1) mL of O_2 min^{-1}; in the presence of 5 equiv, 0.5(1) mL of O_2 min^{-1}).

To try to understand which redox species are involved in this activity, the reaction was followed by EPR spectroscopy and electrospray mass spectrometry (ESMS). Figure 8 presents the EPR spectra recorded before and 20 s after addition of H_2O_2 for **2** and **5**. The EPR spectra recorded for **3** during the reaction closely match those for **5**. The spectra of **2** (Figure 8a) and **5** (Figure 8b) were recorded in the reaction medium acetonitrile which has glassing properties, explaining the poor resolution of the spectra. Nevertheless, their characteristic features are clearly apparent: **2** exhibits the features at low field and the broad line at $g \sim 2$ usually observed for dimanganese(II) species, and **5** presents the 16-line hyperfine pattern on the $g \sim 2$ absorption. After addition of H_2O_2 both spectra are significantly altered and complex and resemble each other. The spectroscopic signature of at least four different species can be found: a mononuclear Mn^{II} species with a six-line spectrum, **2, 5,** and more observable in Figure 8c a bump at 5000 G which can be tentatively associated to a dimanganese(II,III) species since these species have wider spectra around $g \sim 2$ than the other ones.[61] The spectroscopic differences between the reaction mixture

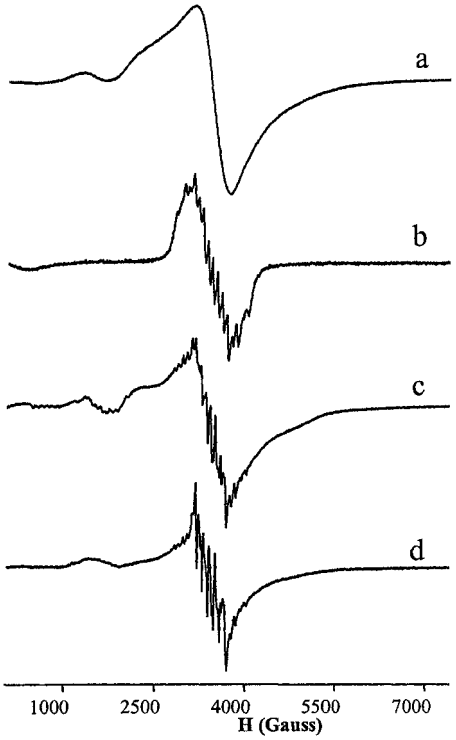

Figure 8. EPR spectra of **2** and **5** recorded before (a, b) and 20 s after (c, d) addition of 50 μL of 9.91 M H_2O_2 to an acetonitrile solution of complex : [complex] = 1 mM in CH_3CN; [H_2O_2] = 250 mM; T = 273 K. EPR conditions : T = 10 K ; P = 0.2 mW; frequency = 9 GHz.

originating from **2** and **5** reside in different proportions of these four species. In addition it is worth noting that in the case of **2** but not **5** the overall intensity of the EPR spectrum decreases by a factor of 2 upon addition of H_2O_2 and then increases during the reaction again by a factor of 2.

A similar monitoring of the reaction with ESMS failed to identify positively the active species. Nevertheless it gave valuable indications on some aspects of the reaction. The starting complex **2** is characterized by a peak at *m*/*e* 741 corresponding to the monocation $[Mn_2(\mu\text{-}O_2CCH_3)_3(bpea)_2]^+$ and its decomposition satellites at *m*/*e* 514 (loss of bpea) and 341 (loss of $Mn(\mu\text{-}O_2CCH_3)_2(bpea)$). In the presence of H_2O_2, two peaks appear at *m*/*e* 327.5, corresponding to **5,** and at *m*/*e* 711, which is associated to oxidation chemistry. The peak at *m*/*e* 711 is assigned to the species $[Mn_2(\mu\text{-}O_2CCH_3)_3(bpea)(bpi)]^+$, which derives from the starting complex by loss of an ethane fragment leading to a degraded bpea ligand possessing an imine function (bpi; Chart 1). This species is observed only in the presence of H_2O_2 and may constitute the initial product in the degradation of the catalysts.

Discussion

Solid-State Properties. A few tricarboxylate-bridged manganese complexes have been reported so far which separate in two distinct structural types according to the bridging mode of the carboxylate groups: in the first type, the three carboxylates adopt the $\mu_{1,3}$ mode,[42,43,46] while one carboxylate is $\mu_{1,1}$ and the two other carboxylates are $\mu_{1,3}$ in the second type.[43−45,47] As a direct consequence of this structural difference, the intermanganese distances are shorter in the second type (3.498 to 3.753 Å) than in the first one (3.688 to 4.034 Å). **2** belongs to the first type, and with a Mn−Mn distance of 3.915 Å, it is closer to the triazacyclononane and to the Tp^{iPr_2} complexes (4.034[42] and 4.006 Å,[46] respectively) than to the bipyridyl one (3.688 Å).[43] This evolution of the intermanganese distance is related to two different structural features. First, the triazacyclononane, the Tp^{iPr_2} and the bpea complexes involve six-coordinate manganese ions while pentacoordinate manganeses are present in the bipy compound resulting in shorter Mn−O(carboxylate) bonds in the latter as expected. Second, and more importantly, there is a twisting of the carboxylate bridges with respect to the Mn−Mn axis which increases from the triazacyclononane to the bpea to the bpy complex, and the larger this twisting the shorter the Mn−Mn distance, as expected.

Chart 1

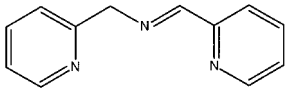

The magnetic exchange interaction in **2** is $-J = 1.3$ cm^{-1}. This value is intermediate between those of the bipy complex ($-J = 0.2$ cm^{-1}) and of the triazacyclononane ($-J = 1.75$ cm^{-1}). The trend in the magnitude of $-J$ is inversely parallel to the Mn−Mn distance: this is reasonable since the more planar the Mn−$\mu_{1,3}$-carboxylate−Mn unit, the longer the Mn−Mn distance and the stronger the overlap between the magnetic orbitals and therefore the antiferromagnetic interaction.

Redox Properties. Up to now, the dimanganese complexes containing the tridentate facially ligands bpea[54−57] and the analogous MeL[51−53] with chelate ring asymmetry (MeL = (2-pyridylmethyl)(2-pyridylethyl)methylamine) have been only isolated at the (III,III), (IV,IV), or (III,IV) oxidation states with the $\{(\mu\text{-}O)(\mu\text{-}O_2CCH_3)_2\}$ and $\{(\mu\text{-}O)_2(\mu\text{-}O_2CCH_3)\}$ core structures. Moreover, the studies of the electrochemical properties of the bpea[40] and the MeL[51−53] complexes have shown that the oxidations of the dimanganese complexes (III,III) are bielectronic and yield quantitatively the (IV,IV) complexes by substitution of an acetate group by an oxo group. The chemical isolation of the dimanganese(II,II) complex in the bpea series with the $\{(\mu\text{-}O_2CCH_3)_3\}$ core structure has allowed us an opportunity to systematically investigate the redox properties of three different cores $\{Mn^{II}_2(\mu\text{-}O_2CCH_3)_3\}$, $\{Mn^{III}_2(\mu\text{-}O)(\mu\text{-}O_2CCH_3)_2\}$, and $\{Mn^{IV}_2(\mu\text{-}O)_2(\mu\text{-}O_2CCH_3)\}$ or $\{Mn^{III}Mn^{IV}(\mu\text{-}O)_2(\mu\text{-}O_2CCH_3)\}$ with the same terminal ligand and study possible core interconversions between the various oxidation levels of manganese. Indeed, the oxidation of the $Mn^{II}_2(\mu\text{-}O_2CCH_3)_3$ complex, **2,** is irreversible and leads mainly to the $Mn^{III}_2(\mu\text{-}O)(\mu\text{-}O_2CCH_3)_2$ complex, **3**. A further oxidation of **3** yields quantitatively the $Mn^{IV}_2(\mu\text{-}O)_2(\mu\text{-}O_2CCH_3)$ complex, **4**. As shown by the shape of the CV of **2** and **3**, the

(61) Zhang, M.; Khangulov, S. V.; Dismukes, G. C.; Barynin, V. V. *Inorg. Chem.* **1994**, *33*, 382.

rate of the electroinduced transformation of **2** into **3** is faster than that observed for **3** into **4**, attesting the great unstability of a $(\mu\text{-}O_2CCH_3)_3$ species at the manganese(III) oxidation level. Moreover, **3** and **4** can be generated selectively because the two two-electron oxidation steps are clearly separated due to the difference observed for the oxidation potentials of **2** and **3** (0.45 and 0.84 V vs Ag/Ag^+ (10 mM)), respectively. In an other way, the value of the reversible system corresponding to the couple $Mn^{IV}{}_2(\mu\text{-}O)_2(\mu\text{-}O_2CCH_3)$/$Mn^{III}Mn^{IV}(\mu\text{-}O)_2(\mu\text{-}O_2CCH_3)$ (**4**/**5**) of 0.61 V is located at a potential between the irreversible oxidations of **2** and **3**. These transformations are chemically reversible by reduction processes, although the two steps are not separated. Indeed, **2** is directly and entirely regenerated by reduction of **4**. **3** cannot be regenerated selectively by reduction of **4** (or **5**) since the reduction potentials of **3** and **4** (or **5**) are too close.

These core interconversions under oxidative and reductive conditions are obviously concomitant with protonation/deprotonation reactions at the bridging oxo groups.

Reactivity. The catalase-like activity of **2**, **3**, and **5** has been monitored by mass spectrometry and EPR and UV−visible spectroscopies, but none of these techniques has provided a clear identification of the active species. Nevertheless, both spectroscopies show that the same species are present during the catalysis reaction although some differences can be noted. From EPR spectroscopy, it appears that mononuclear Mn^{II} and $Mn^{III}Mn^{IV}$ species are present in all reaction mixtures but in higher amounts in those originating from **3** and **5,** which exhibit the lowest activity. Conversely, these reaction mixtures exhibit a smaller amount of binuclear $Mn^{II}Mn^{II}$ species compared to those of **2** which are more active. This suggests that the binuclear $Mn^{II}Mn^{II}$ species can be an active form while the Mn^{II} and $Mn^{III}Mn^{IV}$ species might be degradation products. This is in line with the known poor abilities of the latter kinds of species to disproportionate H_2O_2 while the binuclear $Mn^{II}Mn^{II}$ form is generally active.[31]

UV−visible monitoring during catalysis shows that the solution spectra are dominated by several absorptions near 480 and 570 nm with extinction coefficients of ca. 500 $L{\cdot}mol^{-1}{\cdot}cm^{-1}$. Such absorptions are characteristic of oxo-bridged dimanganese(III) compounds.[62] Indeed, isolated Mn^{III} ions have low intensity absorptions at ca. 500 nm and the presence of intense absorptions in this region is associated with oxo to Mn^{III} charge-transfer transitions. Moreover, when **2** is the starting compound, the overall intensity is lower than with **3** and **5**. The same is true for EPR spectroscopy, which shows a loss of intensity in the case of **2** at the beginning of the reaction and an increase when the reaction subsides. Therefore, the highest activity observed in the case of **2** is correlated with a loss of intensity in both EPR and UV−visible spectroscopies. These observations are consistent with the occurrence of a dimanganese(III) species lacking an oxo bridge. Indeed, formation of such a species would lower the overall intensity of the absorption spectrum. In addition, owing to its even spin state ($S = 2$) the Mn^{III} ion is not easy to detect by EPR and the possible occurrence of antiferromagnetic interactions mediated by acetato bridges makes this detection even more unlikely.

Although no positive evidence for an active species has been obtained in the case of **2**, all the observations made so far are consistent with the occurrence of an active system shuttling between $Mn^{II}Mn^{II}$ and $Mn^{III}Mn^{III}$ states, the latter not involving an oxo bridge. The lower reactivity of **3** and **5** with respect to **2** can originate either from a different mechanism or by a lower concentration of the active species. One could envisage that **3** reacts in the same way as **2**, being oxidized by H_2O_2 into a dimanganese(IV) compound with a single acetate bridge. As a consequence of both the higher oxidation potential of **3** and its weaker tendancy to lose an acetate bridge upon oxidation, this process should be slower than with **2**, in line with the observed lower activity of **3**. Alternatively, reduction of **3** by H_2O_2 could produce a dimanganese(II) species and give rise to the disproportionation reaction. The similarities of both the EPR and UV−visible spectra recorded during the reaction of all compounds support this hypothesis which is reinforced by the observation (Figure 8d) that a dimanganese(II) is formed when starting from **5** (and **3**). The difference in activity between **2** and **3** and **5** could therefore be attributed to differences in producing the actual catalysts, and the absence of oxo bridge in **2** appears to have a positive effect.

As shown by the electrochemical study, an oxo-bridged $Mn^{III}Mn^{III}$ such as **3** is likely to be formed upon an acetate−oxo exchange associated with a two-electron oxidation, and such a process would compete with the disproportionation reaction. In this respect, it is noteworthy that, for the disproportionation of a second batch of H_2O_2, a solution of **2** exhibits the same activity as **3**, suggesting therefore that **3** is formed in the conditions of the disproportionation reaction.

Scheme 2 incorporates all available evidence into a possible mechanism explaining the reactivity of **2** and its transformation in **3**. It is worth noting that in the three compounds the manganese ions are hexacoordinated and therefore the complex must dissociate a ligand to react with H_2O_2 in an inner-sphere process leading to its disproportionation. In all present complexes, acetate is the ligand most likely to be dissociated. The inhibitory effect of acetate on the reactivity of **2** supports this view. It is likely that **2** more readily dissociates acetate than **3** and **5** because of the lower oxidation state of the manganese ions and the lower charge of the core cation. Thus, H_2O_2 should easily oxidize **2** by an inner-sphere two-electron process to give a dihydroxodimanganese(III) with the release of an acetate bridge. The dihydroxodimanganese(III) compound could itself be reduced by H_2O_2 to give O_2 and the corresponding diaquadimanganese(II) species with the release of H_2O. The dihydroxodimanganese(III) compound is the central piece of this mechanism. It is likely to be EPR silent in X-band EPR normal mode, and its formation could account for the loss of intensity in the EPR spectra when **2** is reacted with H_2O_2. This complex should easily loose a water molecule to give **3** in a process competitive with its reduction by H_2O_2.

(62) Gamelin, D.; Kirk, M.; Stemmler, T.; Pal, S.; Armstrong, W.; Penner-Hahn, J.; Solomon, E. *J. Am. Chem. Soc.* **1994**, *116*, 2392.

Scheme 2

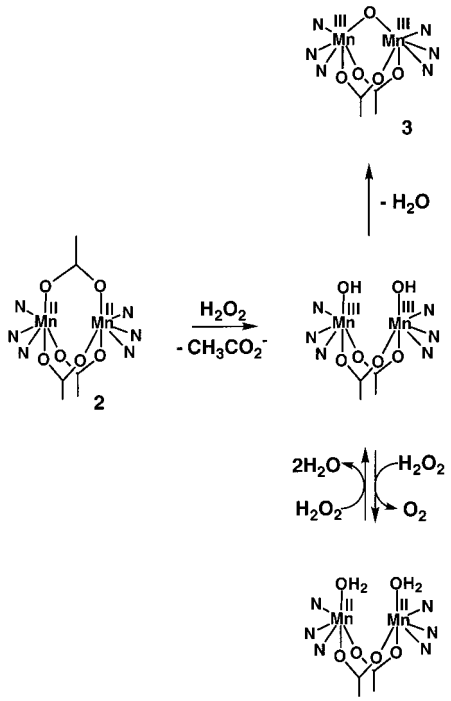

Complete bleaching of the solution at the end of the reaction points to the major formation of manganese(II) species, which are probably mononuclear according to EPR analysis. While the exact nature of this species was not investigated, it is possible that it be a Mn(II) complex of bpi, the imine ligand derived by ethane abstraction from bpea.

Conclusion. This study demonstrates that it is possible to obtain chemically and/or to generate electrochemically dimanganese complexes containing the tridentate ligand bpea at various oxidation levels, (II,II), (III,III), and (IV,IV), and its reduced (III,IV) form without modifying dramatically the overall structure of these dimers. Indeed, all the complexes are triply bridged, and the number of bridging oxo/acetate groups is directly in correlation with the oxidation states of the manganese. Increasing the number of oxo groups from 0 to 1 and from 1 to 2 stabilizes the oxidation states of the manganese from (II,II) to (III,III) and (III,III) to (IV,IV) or (III,IV), respectively. So, it appears that a two electron oxidation involves the substitution of an acetate group by an oxo one. These core interconversions have been also evidenced by electrochemical processes. Furthermore, the three complexes with the $\{Mn^{II}_2(\mu\text{-}O_2CCH_3)_3\}$, $\{Mn^{III}_2(\mu\text{-}O)(\mu\text{-}O_2CCH_3)_2\}$, and $\{Mn^{III}Mn^{IV}(\mu\text{-}O)_2(\mu\text{-}OCCH_3)\}$ core structures disproportionate H_2O_2 and $\{Mn^{II}_2(\mu\text{-}O_2CCH_3)_3\}$ is far more active than the two others. During the catalysis, we observed that the same species are present in the reaction mixtures after a while, albeit in slightly different proportions. As revealed by the electrochemical study, this is a consequence of the ability of the tris(acetato) structure to lead successively by oxidation to a bis(acetato) and a mono(acetato) one.

Acknowledgment. I.R. thanks the CNRS for financial support.

Supporting Information Available: Scheme S1, showing the electrochemical properties of complex **2,** and X-ray crystallographic details for complexes **1** and **2** in CIF format. This material is available free of charge via the Internet at http://pubs.acs.org.

IC010721E